Flow, Turbulence and Combustion (2021) 106:405–417
https://doi.org/10.1007/s10494-020-00122-4

# Dense Sprays with a Focus on Atomization and Turbulent Combustion

**G. Singh[1] · A. Kourmatzis[1] · A. R. Masri[1]**

Received: 26 November 2019 / Accepted: 16 March 2020 / Published online: 26 March 2020
© Springer Nature B.V. 2020

**Abstract**
This paper presents a brief overview of recent research conducted by our group to advance current understanding of primary and secondary atomization as well as the turbulent combustion of sprays. The focus is on air-blast atomization. The burner employed exploits the benefit of recessing a liquid-injecting needle into the primary air-blast annulus to transition the spray exiting the burner from dilute to dense. A pilot is used to stabilize the flame to the burner which is sitting in a co-flowing stream of secondary air. Direct links are found between the wave instabilities and the size of the fragments shed from the liquid core. In the secondary atomization zone, the statistics of three types of fragments, namely droplets, ligaments and irregular fluid shapes are provided. This approach may provide a platform for the modelling of denser spray flames without the need to account for primary atomization. For reacting cases, mean temperature measurements are presented. This burner (referred to as the needle spray burner) is employed to stabilize dilute and dense spray flames.

**Keywords** Air-blast sprays · Surface instabilities · Primary atomization · Secondary atomization · Turbulent combustion

## 1 Introduction

The applications of spray flows span a very broad spectrum far beyond the immediate concern of this paper which is more directed towards combustion. Targeted spraying in agriculture, drug delivery in pharmaceuticals, spray drying of food products and fire suppression are samples of key applications that would benefit from an improved understanding of spray atomization and control of droplet dynamics. It is precisely such refined control of both droplet formation and size distribution that remain a challenge despite recent progress in this field (Faeth et al. 1995; Gounder et al. 2012; Kourmatzis et al. 2013; Lasheras et al. 1998; Lowe et al. 2017; Shinjo and Umemura 2010; Dumouchel 2008). This is relevant to all modes of liquid atomization which include air-blast and pressure atomization as well as

✉ A. R. Masri
assaad.masri@sydney.edu.au

[1] School of Aerospace, Mechanical and Mechatronic Engineering, The University of Sydney, Sydney, NSW 2006, Australia

other less common modes such as electrostatic atomization (Kourmatzis and Shrimpton 2009; Shrimpton 2009), flow blurring (Jiang and Agrawal 2015; Simmons and Agrawal 2012; Gañán-Calvo and Barrero 1999), and effervescent atomization (Kourmatzis et al. 2016; Sovani et al. 2001).

It is well established that in sprays, the droplet size downstream of the liquid injection point is largely controlled by upstream conditions where the primary and secondary break-up of the liquid occurs. The key dimensionless numbers that characterize both stages of break-up are the Weber, Ohnesorge and Reynolds numbers and regime diagrams have been developed with respect to these dimensionless numbers for both primary (Faeth et al. 1995; Kourmatzis and Masri 2015; Marmottant and Villermaux 2004; Varga et al. 2003; Shinjo and Umemura 2010; Lasheras et al. 1998; Lasheras and Hopfinger 2000), and secondary atomization (Faeth et al. 1995; Gounder et al. 2012; Guildenbecher et al. 2009; Kourmatzis et al. 2015; Lowe et al. 2017). Other parameters such as gas-to-liquid ratio, turbulence levels and the role (and type) of instabilities remain vague at best. Marmottant and Villermaux (2004) have provided excellent insights into the role of instabilities in the formation of fluid fragments. Their findings are reflected in the subsequent correlations developed by Varga et al. (2003) linking such instabilities to the size distribution of droplets. Extending this work through detailed imaging of instabilities, fragments, and droplets over a range of fuels and atomization conditions is a key objective of research undertaken by the combustion research group at the University of Sydney (Kourmatzis and Masri 2014, 2015; Kourmatzis et al. 2013, 2015; Lowe et al. 2017; Gounder 2009).

Turbulent combustion of sprays occurs in the vapor cloud that surrounds either single droplets or a cluster of droplets and the transition between these modes may be characterized by the Group number developed by Chiu and Liu (1977). Joint imaging of heat release zones (from joint LIF-OH-CH2O) and droplets (from Mie scattering) in turbulent dilute sprays flames of ethanol have shown both single droplet as well as group combustion may be detected in such flames (Chiu and Liu 1977; Gounder 2009; Juddoo and Masri 2011). Regardless, combustion in turbulent sprays must involve mixed-modes due to the continuous injection of fuel vapor from the evaporating droplets. Mixed-mode combustion refers here to the possible co-existence of diffusion, premixed, partially premixed and stratified flames within the same region (Chigier 1983; Faeth 1996; Chiu and Liu 1977). This, in addition to the relevant interaction with chemical kinetics, poses a serious challenge to models which are limited to single modes (Chigier 1983; Faeth 1996). The development of generalized models for mixed-mode combustion remains a challenge yet highly relevant for practical combustors as well as for the more dense spray flames studied here.

This paper provides a brief overview of recent progress in our current understanding of atomization and the combustion of turbulent, moderately-dense spray jets and flames. It focuses on a selected air-blast configuration that is found to be relevant for enhancing the fundamental understanding of atomization and combustion. While this is necessary for brevity, it leaves out many other spray burner configurations (Tyliszczak et al. 2014; Shum-Kivan et al. 2017; Verdier et al. 2017), important aspects of sprays such as spray penetration and combustion in engines (Turns 2012; Pham et al. 2014), and recent advances in direct numerical simulations (Salehi et al. 2016; Galindo et al. 2017; Salehi et al. 2017; Jenny et al. 2012; Echekki and Mastorakos 2011). This paper evolves as follows: After a brief introduction to the Sydney needle spray burner, the next section discusses primary atomization with a focus on the evolution of instabilities and their link to the break-up of the liquid core and the shedding of fluid fragments. The following section is concerned with secondary atomization and the disintegration of filaments and other fluid fragments into droplets. Statistics of each category are presented. The results presented in

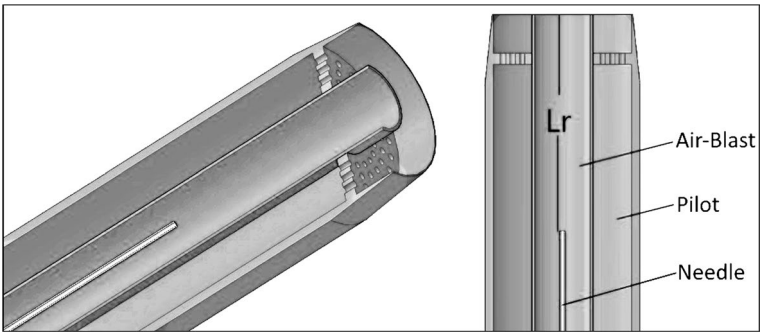


**Fig. 1** Cut section of the burner top, showing pilot, air-blast, and needle jet

**Table 1** Relevant case details

| Case | $d_{jet}$ (mm) | D (mm) | Q (g/min) | $U_{jet}$ | $U_{gas}$ | $Re_{jet}$ | $Re_{gas}$ | We | MFR |
|---|---|---|---|---|---|---|---|---|---|
| N27-AS13-00 | 0.21 | 10 | 3 | 1.8 | 88 | 910 | 56088 | 88 | 0.01 |
| N19-AS02-XX | 0.686 | 10 | 75 | 4.3 | 36 | 6967 | 21281 | 35 | 0.37 |
| N19-AS06-XX | 0.686 | 10 | 45 | 2.6 | 36 | 4180 | 21281 | 39 | 0.22 |
| N19-AS07-XX | 0.686 | 10 | 75 | 4.3 | 60 | 6967 | 35468 | 108 | 0.22 |
| N19-AS08-XX | 0.686 | 10 | 45 | 2.6 | 48 | 4180 | 28374 | 72 | 0.17 |

the previous two sections originate mainly from back-lit, microscopic high-speed imaging. The final section presents recent results from turbulent combustion of dilute and dense sprays stabilized on the Sydney needle spray burner which is now adopted as a modelling platform for advancing modelling efforts by the International Workshop on the Turbulent Combustion of Sprays (TCS).

## 2 Burner and Selected Cases

A schematic of the atomizer/burner selected for these studies (referred to as the Sydney needle spray burner) is shown in Fig. 1. Full details are given elsewhere (Lowe et al. 2017) and only a very brief description is given here. Liquid issues from a needle into the surrounding air-blast stream with a diameter D = 10 mm. The needle can be recessed into the air-blast stream up to 80 mm upstream of the jet exit plane so that the issuing spray can transition from dense to dilute. For studies of primary atomization, the recess distance is kept at Lr = 0 mm, so that the liquid core is exposed. The air-blast is located within a pilot stream, 25 mm in diameter (employed only for the reacting cases) and the entire burner assembly is located within a co-flowing air stream. Two needle sizes are employed here, namely N27 and N19 with internal diameters of 0.21 and 0.686 mm, respectively. The cases studied are documented in Table 1. The naming terminology is explained with reference to: N27-AS13-00 where N27 refers to the needle size, A = acetone, S for non-reacting sprays (so the reacting acetone case would be referred to as AF), 13 is the case number and last two digits refer to a recess distance Lr, where this is retained as xx implies

that the case may involve more than one Lr). In Table 1, We is the Weber number defined as "$We = \rho_a(U_a - U_l)^2 d)/\sigma_l$ , and MFR refers to the mass flux ratio of air-blast over liquid. The Reynolds number for the liquid jet ($Re_{jet}$) and the gas ($Re_{gas}$) are respectively based on the diameters of the needle and the air blast streams. The N27 needle, owing to its small diameter, allows investigation of jet instabilities and fragment formation from a single image frame. Therefore, the same is used here to investigate primary atomization. The N19 cases have been discussed in-length previously (Lowe et al. 2017, 2019a, b; Lowe 2018), with further results presented here focusing on the atomization region.

The reader should note that the axial locations of the spray are presented as 'x/D', where 'x' is the distance from the burner exit and 'D' is the air-blast tube diameter. For microscopic imaging results 'x' represents the axial distance between burner exit and bottom of the image, and for temperature results, it represents the axial distance between thermocouple end and burner exit. For all the results presented here, results at x/D = 0 denote a distance of 1.3 mm from the burner exit. This is a physical limitation which is necessary to avoid excessive light scattering from the tube wall.

## 3 Primary Atomization

Primary atomization refers to the initial shedding of fragments from a continuous liquid core. This region is marked by the initial formation of instabilities which grow on the liquid surface. Break-up of the liquid core is another key parameter which marks the nominal transition to secondary break-up. This section presents results from on-going research aimed at resolving the complexities of these phenomena. High-speed back-lit imaging has formed the main diagnostics platform for both primary and secondary atomization and a brief description of the latest evolution of this technique is presented followed by some sample data that sheds light about the links between initial instabilities, jet break-up, and the shedding of liquid fragments.

The images obtained from the high-speed imaging are binarized using a carefully chosen background threshold. For all the cases, 2000 images are collected at several axial locations of the spray. Each binarized image has a size of 3.4 × 3.4 mm, and an image resolution of 4.5 μm/pixel. The images are processed to obtain wavelength and amplitude of instabilities as well as fragment statistics. For a detailed description of the image processing technique, the reader is directed elsewhere (Kourmatzis et al. 2015; Lowe et al. 2017). In this paper the liquid fragments are classified into three major categories based on their aspect ratio (AR) and size ($d_{10}$), as follows: Droplets ($AR < 3$ & $d_{10} < d_{jet}$), Ligaments ($AR > 3$ & $d_{10} > d_{jet}$), and the remaining large atomizing-objects are named as Unbroken Bodies (UnB). This classification approach has shown physical consistency with the literature (Kourmatzis et al. 2013, 2015; Lowe et al. 2017) on spray structure, and hence the same is adapted here. The definition of wavelength and amplitude of the instability is shown in Fig. 2a.

In Case AS13, the spray is generated using a small needle (N27, $d_{jet}$ = 0.21 mm), while the air-blast diameter is kept same (D = 10 mm); and owing to the high Weber number (We = 80), the liquid jet breaks within single image frame. Therefore, Case AS13 is employed here to simultaneously analyze the growth of jet instabilities and their link to fragment size. Figure 2a shows the snapshot of a liquid jet (at x/D = 0) shedding a ligament that has its major axis similar to the wavelength of the jet instability. The high-speed air, surrounding the jet, initiates surface perturbations that grow in both wavelength and

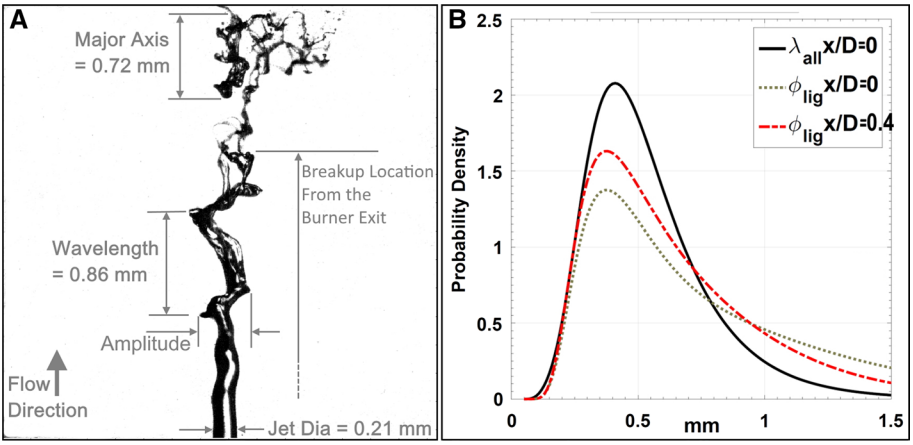


**Fig. 2** **a** Snapshot of the jet at x/D = 0 for spray AS13 showing the wavelength of the instability and sizes of the broken liquid fragment (left). **b** Probability density distribution of wavelength of the jet instabilities and major axis of the ligaments at x/D = 0 & 0.4 (right). The figure is a continuation of the work submitted elsewhere (Singh et al. 2020)

amplitude leading to jet breakup which is marked by the end of the continuous liquid core. The location of break-up length is also marked in Fig. 2a. Generally, it is noticed that shedding of liquid fragments is associated with one complete wave whose wavelength is proportional to the size of that fragment. This is consistent with our earlier results (Singh et al. 2020) as well as with other studies linking the size of the ligaments to jet instabilities (Faeth 1996; Jiang and Agrawal 2015; Juddoo and Masri 2011; Kourmatzis et al. 2016). Here, the wavelength and fragment sizes are measured directly in the same image frame along with the break-up location. The relationship between fragment size and instabilities is discussed by comparing the probability density distribution of instability-wavelength and the major axis of the ligaments. The mean values of wavelength and amplitude, obtained in this work, are validated against the correlations proposed by Marmottant and Villermaux (2004) and Varga et al. (2003), but only pdf distributions are discussed here, for brevity.

Figure 2b shows the probability density distribution of the wavelength of the instabilities and major axis of the ligaments. The pdf of wavelength is shown for x/D = 0 (solid line), while the pdf of size of the ligaments is shown for x/D = 0, and 0.4 (dashed lines). It is observed that the pdf of wavelength is similar to the pdf of the ligament size, and the sizes corresponding to peak of the pdf's are approximately similar. This suggests that most of the ligaments have their major axis similar to the wavelength of instabilities. The difference in pdfs for higher sizes (> 1 mm) could be attributed to the elongation of broken liquid fragments by surrounding high-speed air, and the high Weber number of Case AS13 (We = 80). It is expected that, for low Weber number sprays, the wavelength and fragment size distribution will be similar for the entire size range. Still, the apparent similarity between the pdf of wavelength and major axis of ligaments confirms that the liquid jet breaks into fragments of size proportional to the wavelength of jet instabilities. Similar trends are observed for other cases, but not presented here for brevity.

The jet instabilities, near their initiation, have small wavelength and amplitude. Owing to the aerodynamic effect of the surrounding air-blast, the wavelength and amplitude of the instabilities increase as they grow downstream and this eventually leads to jet breakup,

as shown in Fig. 2a. Here, the growth of the instabilities is discussed in terms of ratio of wavelength and amplitude ($\lambda/a$-ratio) of instabilities. This is done here to study the growth of both wavelength and amplitude simultaneously where the ratio is calculated by dividing wavelength of each instability by its amplitude. Figure 3 shows the joint-histogram of the $\lambda/a$-ratio and the location of the corresponding jet instability for Case AS13. It is observed that the $\lambda/a$-ratio decreases with downstream locations and approaches to $\lambda/a \approx 2$ near jet breakup, (for this case the liquid jet breaks approximately 3 mm from the burner exit). This is consistent with our earlier finding using other needle sizes (Singh et al. 2020). Previously, (Marmottant and Villermaux 2004) have also suggested $\lambda/a \approx 2$ as a threshold for liquid shredding from the jet, however, no direct link between the $\lambda/a$-ratio and jet breakup was reported. Here, the $\lambda/a$-ratio of the growing instabilities and the location of the jet break-up are presented in conjunction confirming the relevance of $\lambda/a \approx 2$ as a threshold leading to jet breakup. Similar trends are observed for all other cases, but not presented here for brevity.

## 4 Secondary Atomization

The previous section discussed the characteristics of surface instabilities in terms of jet breakup, and their relation to fragment size. The liquid fragment formed after jet breakup further atomizes into small ligaments and large droplets, and finally into very small droplets in the downstream region of the spray. This process is known as secondary atomization. Previously, such sprays have been categorized into three regions based on liquid density as dense, intermediate, and dilute region (Kourmatzis et al. 2015; Lowe et al. 2017). The dense region is the near-field region consisting of the dense liquid core and large liquid objects formed from jet breakup. The dilute region is the far-field region where droplet-droplet interactions are minimal, and the intermediate region is between these two zones, where droplet-droplet interactions are common (Kourmatzis et al. 2015; Lowe et al. 2017; Guildenbecher et al. 2009). The spray structure in the intermediate region is generally

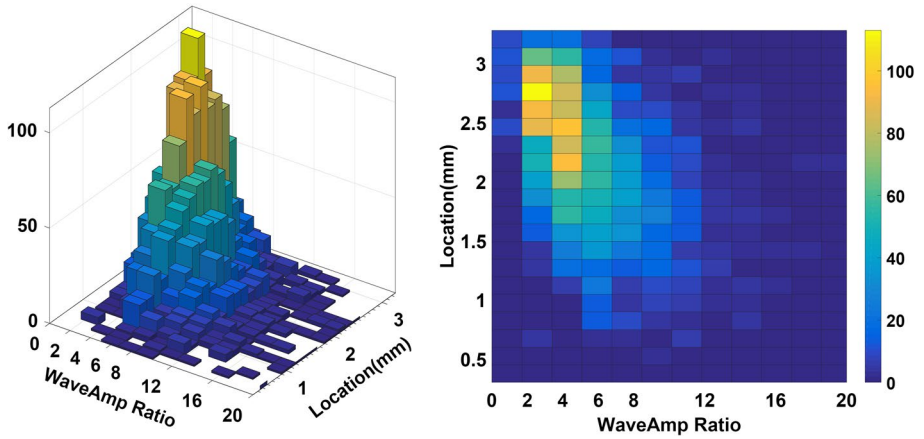


**Fig. 3** Histogram of ratio of wavelength and amplitude of instabilities with respect to their location, for Case AS13. Left plot shows the histogram, right plot shows the top view of the histogram. The figure is a continuation of the work submitted elsewhere (Singh et al. 2020)

dictated by secondary atomization and is of paramount importance, as it determines the downstream combustion characteristics of the spray. Therefore, this section will discuss the spray structure in the intermediate region in terms of spray area fraction, and fragment statistics of droplets, ligaments, and unbroken bodies.

Figure 4 shows the average liquid fraction (normalized by jet area) at the centreline of the spray for several axial locations of Cases AS2, AS6, AS7, and AS8. This is calculated by superimposing the 2000 images collected, and dividing the total number of pixels covered by the spray (in 2000 images) by the total number of pixels covered by the jet (in 2000 images), at the centerline. This normalized liquid fraction represents, therefore, the probability of presence of spray at the spray location of interest. It is interesting to note that the rate of decay of liquid fraction is different for all the cases, and is a function of the mass flux ratio. Case AS8 has the lowest mass flux ratio, and the highest decay rate while cases AS6 and AS7 have similar mass flux ratios, and hence the area decays at a similar rate. Case AS2 has the highest mass flux ratio and therefore the decay rate is the lowest. This indicates that, other than spray dispersion, the mass flux ratio is a key controlling parameter. The next part will discuss the mechanism or range of mechanisms governing the atomization of individual liquid fragments.

Figure 5 presents the normalized area of the individual liquid objects, droplets, ligaments, unbroken bodies, and liquid jet for Cases AS2 and AS8 plotted against the distance from the needle tip (x*/D). This is to distinguish it from x which is the distance from the jet exit plane such that $x^* = x + Lr$. The object area represents the average number of pixels covered by droplets, ligaments, and unbroken bodies (in 2000 images). In Fig. 5, the object area is normalized by the image size (768 × 768 pixels). For Case AS2, the area of the jet increases first with axial location owing to jet fluctuations; and starts to decrease after jet breakup. Simultaneously, an increase in area of the unbroken bodies & ligaments is observed, due to formation of ligaments and unbroken bodies from the jet breakup—the intersection of the area profile of jet and unbroken bodies (indicated by arrow) represents the approximate jet breakup location. With downstream location, the ligaments and unbroken bodies atomize into droplets leading to an increase in droplet area and decrease in the area of unbroken bodies & ligaments. It is interesting to note that the area of all three objects droplets, ligaments, and unbroken

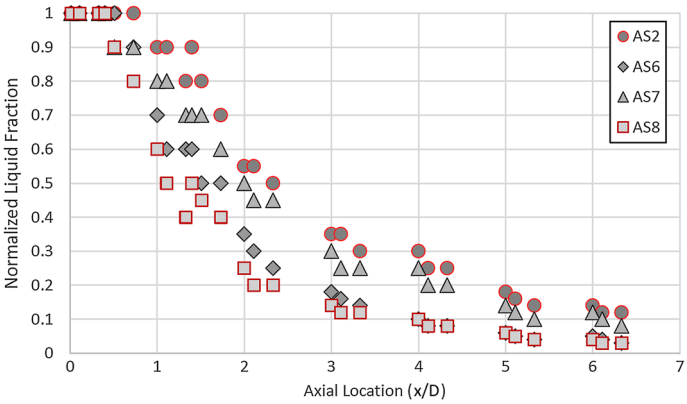


**Fig. 4** Normalized liquid fraction for with respect to axial location for Case AS2, AS6, AS7, and AS8. It is calculated by dividing the total number of pixels covered by the spray (in 2000 images) by the total number of pixels covered by the jet (in 2000 images), at the centreline

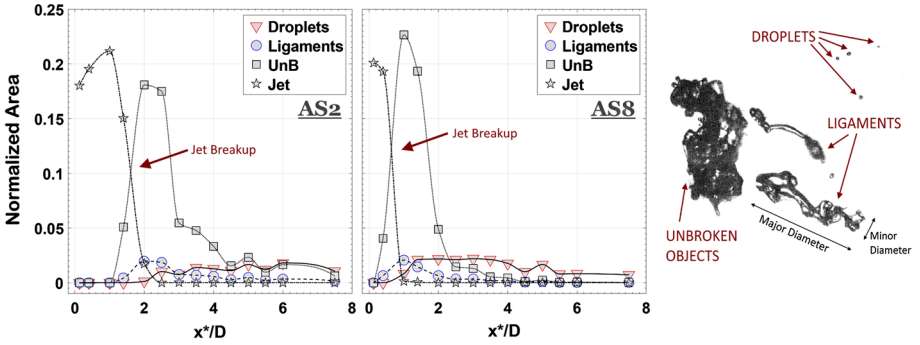


**Fig. 5** Normalized area fraction of liquid fragments (droplets, ligaments, unbroken objects, and liquid jet) with respect to axial location from needle top (x*/D) for Cases AS2 and AS8. The object area represents the average number of pixels covered by individual fragments (in 2000 images). The fragment area is normalized by the image area. The right side shows the definition of classified liquid fragments. The figure is a continuation of the work published elsewhere (Lowe et al. 2017)

bodies becomes similar at x*/D = 7–7.5. Lowe et. al. (2017) has reported that this location corresponds to the completion of the secondary atomization process. For Case AS8, the object area follows similar trends but the location corresponding to atomization completion shifts closer to the atomizer exit (x*/D = 2.5–3). The reason for this could be attributed to higher air entrainment (indicated by a low mass flux ratio) for Case AS8. This implies that the liquid fragment atomizes at a faster rate in Case AS8, as compared to Case AS2, and this leads to an early completion of atomization. Similar trends are observed for other cases, but not presented here for brevity.

Figure 6 presents the object count of droplets, ligaments, and unbroken bodies as a function of their size for Cases AS2 and AS8, for two axial locations corresponding to x/D = 0 and 5. For these cases, the needle is recessed at Lr = 25 mm from the burner exit and thus x/D = 0 and 5 are similar to x*/D = 2.5 and 7.5, respectively (note that x* = x + Lr). It is noticed that at x*/D = 2.5, the mean droplet size (solid line) is similar for Cases AS2 and AS8. However, the droplet count (in %) is lower, and the object count and size of ligaments and unbroken bodies are higher for case AS2 as compared to Case AS8. This suggests that the percentage of completely atomized objects is higher for Case AS8 as compared to Case AS2, and confirms that the atomization rate is higher for Case AS8. This validates the previous assertion that the high air entrainment leads to a more rapid atomization of liquid fragments. With downstream location (x*/D = 5), the number of droplets increases and the object count of ligament as well as unbroken bodies decrease for both Cases AS2 and AS8. This is expected since, on moving downstream, the atomization of ligaments and unbroken bodies leads to formation of droplets, which increases the number of droplets, and subsequently decreases the number of ligaments and unbroken bodies. The correlation between unbroken bodies and ligaments is not analysed here, as it will involve time tracking of individual fragments at several axial locations of spray, which is outside the scope of this work.

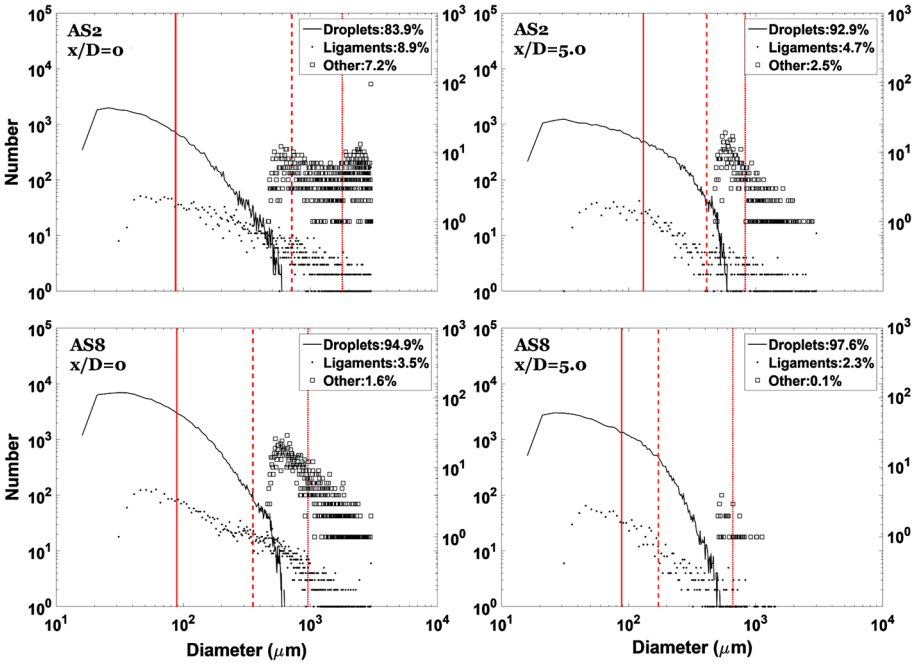


**Fig. 6** Number density of liquid fragments with respect to their size (d10) for cases AS2, and AS8 at x/D location of 0.13 and 5.0. The needle is at recess length of 25 mm, which corresponds to x*/D of 2.5, and 7.5, respectively. The figure is a continuation of the work published elsewhere (Lowe et al. 2017)

## 5 Turbulent Combustion of Sprays

This section discusses the characteristics of reacting sprays in terms of flame stability and mean temperature profiles measured at several axial and radial locations of the spray. Figure 7 shows sample images of flames and the stability limits plotted for the N19 needle and for acetone fuel. The stability limits show the velocity at which the flame blows-off

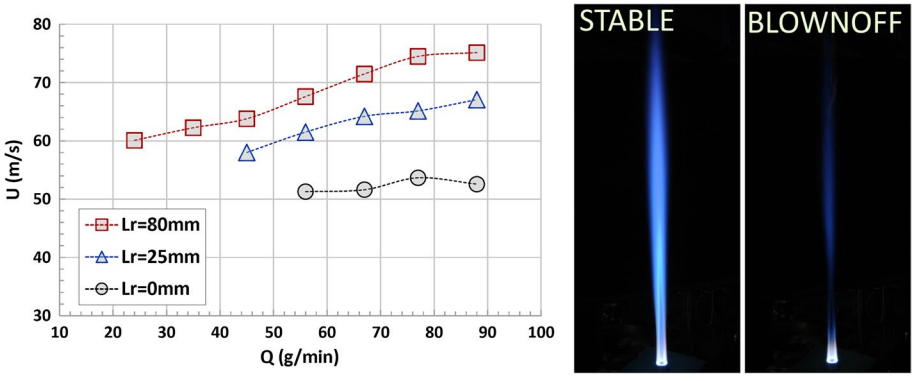


**Fig. 7** Blow-off air-blast velocity (U) for acetone fuel at different recess length (Lr) plotted against the fuel loading (Q). The two images at the right shows the snapshot of stable and blown off flame

downstream of the pilot versus fuel loading for different recess distances. This is done here to compare the results presented here with the previously reported stability limits for the same burner, elsewhere (Lowe et al. 2017; Lowe 2018). It is evident that the flame stability is affected by the recess length (Lr) and hence by the quality of the spray. For a given liquid loading, and with changing recess from Lr = 0 to 80 mm, the spray transitions from dense to dilute and the flame becomes more stable. A similar behaviour for ethanol fuel is observed but not shown here for brevity. However, biodiesel exhibits two stability limits, an upper one similar to that of ethanol and acetone, and a lower stability limit induced by virtue of the higher viscosity, which lead to fuel droplets dribbling from the central jet to the pilot stream and hence causing an unstable flame.

The temperature results presented here are a mean of 200 data points measured using an R-Type thermocouple. The response time of the thermocouple is 0.01 s, and the standard deviation for each measurement is below 2% of the mean. Figure 8 shows the flame temperature at several axial and radial locations for Cases N19-AF02-25, N19-AF06-25 and N19-AF08-25 (referred to hereon as AF2, AF6, and AF8). The recess length is kept at 25 mm for all the cases. For all the cases, near the center, the liquid fragments are large and are still atomizing, resulting in a low temperature at the centerline (for x/D = 10, 15 and 30). With downstream locations, as the atomization process nears completion, the centerline temperature increases, and the location for peak temperature shifts to the center at x/D = 30. For all the cases, the temperature profile at x/D = 10 is similar, and the peak temperature is observed at a similar radial location owing to the greater influence of the pilot at this axial location. On moving downstream (x/D = 15), while the temperature profiles are similar; the radial location for peak temperature shifts towards the center for Case AF8 and AF6. For Case AF6, the peak temperature occurs at r/D ≈ 0.7 while for Case AF8, it occurs at r/D ≈ 0.5. This could be owing to the faster atomization for case AF8 as it is evident from the fragment statistics shown in Fig. 6. This results in the peak temperature occurring closer to the center for Case AF8 as compared to other cases (due to higher vaporization rate of droplets), at axial locations of x/D = 15 and 20. Further downstream at x/D = 30, as the spray is gradually consumed, the peak temperature occurs closer to the centerline for all the cases. For Case AF2, the centerline temperature at x/D = 30 is higher as compared to Case AF6 and AF8 owing to higher liquid loading (fuel). The results presented in this section, while limited, provide insights into how the spray structure in the intermediate region, governed by secondary atomization, can control the characteristics of the flame. Further imaging of reactive scalars (such as OH and formaldehyde), combined

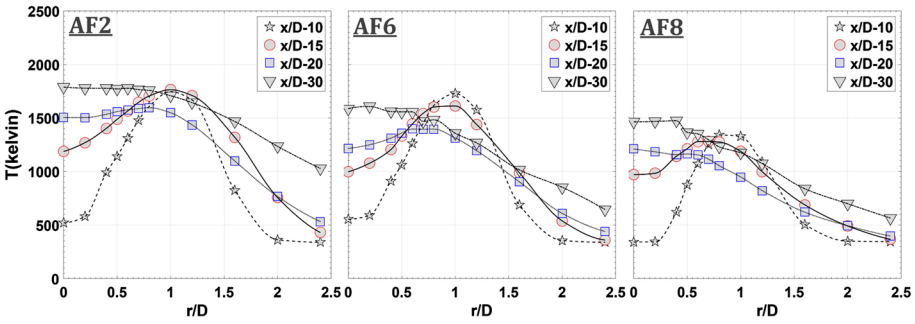


**Fig. 8** Flame temperature at various radial locations at recess length of 25 mm, for cases AF2, AF6, and AF8

with Mie scattering, will be conducted in selected flames to reveal more details about the structure of the reaction zones and their locations with respect to liquid fragments.

## 6 Concluding Remarks

The atomization and turbulent combustion of air-assisted sprays is studied using the Sydney piloted needle spray burner. Microscopic backlit imaging is employed to study primary and secondary atomization. Flames are observed for different liquid loading where the injection needle is recessed so that the spray transitions from dilute to dense. The following conclusions are drawn:

1. Breakup of the liquid core seems to occur when the wavelength/amplitude ($\lambda/a$) ratio of surface instabilities is close to two (($\lambda/a \approx 2$). The size of ligaments shed from the liquid core is also similar to the wavelength of the instabilities which appear to be responsible for the issue of these ligaments.
2. In the secondary atomization region, the analysis of area fraction and fragment statistics revealed that higher air-blast velocities enhance the rate of secondary atomization, and lead to early completion of atomization. The mass flux ratio (MFR) is a key control parameter in the downstream atomization region.
3. Flame stability is directly influenced by the quality of the spray structure at the jet exit plane. This is evident from the varying stability limits for different recess distances. Turbulence-chemistry interactions and possibly mixed-mode combustion appear to affect the flame structure and this will be revealed in future work through more detailed measurements. An early completion of atomization results in a more developed temperature profile closer to the burner exit, as observed for Case N19-AF08-25.

**Acknowledgements** This work is supported by the Australian Research Council.

## Compliance with Ethical Standards

**Conflict of interest** The authors declare that they have no conflict of interest.

## References

Chigier, N.: Group combustion models and laser diagnostic methods in sprays: a review. Combust. Flame **51**(Supplement C), 127–139 (1983). https://doi.org/10.1016/0010-2180(83)90093-7

Chiu, H.H., Liu, T.M.: Group combustion of liquid droplets. Combust. Sci. Technol. **17**(3–4), 127–142 (1977). https://doi.org/10.1080/00102207708946823

Dumouchel, C.: On the experimental investigation on primary atomization of liquid streams. Exp. Fluids **45**(3), 371–422 (2008). https://doi.org/10.1007/s00348-008-0526-0

Echekki, T., Mastorakos, E.: Turbulent combustion modeling: advances, new trends and perspectives. Dordrecht: Springer Netherlands (2011)

Faeth, G.: Spray combustion phenomena. Symp. (Int.) Combust. **26**(1), 1593–1612 (1996). https://doi.org/10.1016/S0082-0784(96)80383-3

Faeth, G., Hsiang, L.P., Wu, P.K.: Structure and breakup properties of sprays. Int. J. Multiph. Flow **21**(Supplement), 99–127 (1995). https://doi.org/10.1016/0301-9322(95)00059-7. **(Annual Reviews in Multiphase Flow 1995)**

Galindo, S., Salehi, F., Cleary, M., Masri, A.: MMC-LES simulations of turbulent piloted flames with varying levels of inlet inhomogeneity. Proc. Combust. Inst. **36**(2), 1759–1766 (2017). https://doi.org/10.1016/j.proci.2016.07.055

Gañán-Calvo, A., Barrero, A.: A novel pneumatic technique to generate steady capillary microjets. J. Aerosol Sci. **30**(1), 117–125 (1999). https://doi.org/10.1016/S0021-8502(98)00029-9

Gounder, J.: An Experimental Investigation of Non-reacting and Reacting Spray Jets. Ph.D. Thesis. The University of Sydney (2009)

Gounder, J.D., Kourmatzis, A., Masri, A.R.: Turbulent piloted dilute spray flames: flow fields and droplet dynamics. Combust. Flame **159**(11), 3372–3397 (2012). https://doi.org/10.1016/j.combustflame.2012.07.014

Guildenbecher, D.R., López-Rivera, C., Sojka, P.E.: Secondary atomization. Exp. Fluids **46**(3), 371 (2009). https://doi.org/10.1007/s00348-008-0593-2

Jenny, P., Roekaerts, D., Beishuizen, N.: Modeling of turbulent dilute spray combustion. Prog. Energy Combust. Sci. **38**(6), 846–887 (2012). https://doi.org/10.1016/j.pecs.2012.07.001

Jiang, L., Agrawal, A.K.: Investigation of glycerol atomization in the near-field of a flow-blurring injector using time-resolved PIV and high-speed visualization. Flow Turbul. Combust. **94**(2), 323–338 (2015). https://doi.org/10.1007/s10494-014-9572-2

Juddoo, M., Masri, A.: High-speed OH-PLIF imaging of extinction and re-ignition in non-premixed flames with various levels of oxygenation. Combust. Flame **158**(5), 902–914 (2011). https://doi.org/10.1016/j.combustflame.2011.02.003

Kourmatzis, A., Masri, A.R.: The influence of gas phase velocity fluctuations on primary atomization and droplet deformation. Exp. Fluids **55**(2), 1659 (2014). https://doi.org/10.1007/s00348-013-1659-3

Kourmatzis, A., Masri, A.R.: Air-assisted atomization of liquid jets in varying levels of turbulence. J. Fluid Mech. **764**, 95–132 (2015). https://doi.org/10.1017/jfm.2014.700

Kourmatzis, A., Shrimpton, J.S.: Electrohydrodynamics and charge injection atomizers: a review of the governing equations and turbulence. At. Sprays **19**(11), 1045–1063 (2009). https://doi.org/10.1016/j.fuel.2013.01.069

Kourmatzis, A., Pham, P., Masri, A.: Air assisted atomization and spray density characterization of ethanol and a range of biodiesels. Fuel **108**(Supplement C), 758–770 (2013). https://doi.org/10.1016/j.fuel.2013.01.069

Kourmatzis, A., Pham, P.X., Masri, A.R.: Characterization of atomization and combustion in moderately dense turbulent spray flames. Combust. Flame **162**(4), 978–996 (2015). https://doi.org/10.1016/j.combustflame.2014.09.021

Kourmatzis, A., Lowe, A., Masri, A.: Combined effervescent and airblast atomization of a liquid jet. Exp. Therm. Fluid Sci. **75**, 66–76 (2016). https://doi.org/10.1016/j.expthermflusci.2016.02.002

Lasheras, J.C., Hopfinger, E.J.: Liquid jet instability and atomization in a coaxial gas stream. Annu. Rev. Fluid Mech. **32**(1), 275–308 (2000). https://doi.org/10.1146/annurev.fluid.32.1.275

Lasheras, J.C., Villermaux, E., Hopfinger, E.J.: Break-up and atomization of a round water jet by a high-speed annular air jet. J. Fluid Mech. **357**, 351–379 (1998). https://doi.org/10.1017/S0022112097008070

Lowe, A.: Flow and Temperature-field Structure of Turbulent Spray Flames: From Dilute to Dense. Ph.D. Thesis. The University of Sydney (2018)

Lowe, A., Kourmatzis, A., Masri, A.R.: Turbulent spray flames of intermediate density: stability and near-field structure. Combust. Flame **176**, 511–520 (2017). https://doi.org/10.1016/j.combustflame.2016.10.024

Lowe, A., Thomas, L., Satija, A., Lucht, R., Masri, A.: Chirped-probe-pulse femtosecond cars thermometry in turbulent spray flames. Proc. Combust. Inst. **37**(2), 1383–1391 (2019a). https://doi.org/10.1016/j.proci.2018.06.149

Lowe, A., Thomas, L.M., Satija, A., Lucht, R.P., Masri, A.R.: Five KHz thermometry in turbulent spray flames using chirped-probe-pulse femtosecond cars, part ii: Structure of reaction zones. Combust. Flame **200**, 417–432 (2019b). https://doi.org/10.1016/j.combustflame.2018.10.034

Marmottant, P., Villermaux, E.: On spray formation. J. Fluid Mech. **498**, 73–111 (2004). https://doi.org/10.1017/S0022112003006529

Pham, P., Bodisco, T., Ristovski, Z., Brown, R., Masri, A.: The influence of fatty acid methyl ester profiles on inter-cycle variability in a heavy duty compression ignition engine. Fuel **116**, 140–150 (2014). https://doi.org/10.1016/j.fuel.2013.07.100

Salehi, F., Cleary, M.J., Masri, A.R.: A sensitivity analysis for sparse-Lagrangian MMC in simulations of a n-dodecane reacting jet. In: SAE Technical Paper. SAE International (2016). https://doi.org/10.4271/2016-01-0859

Salehi, F., Cleary, M., Masri, A., Ge, Y., Klimenko, A.: Sparse-lagrangian MMC simulations of an n-dodecane jet at engine-relevant conditions. Proc. Combust. Inst. **36**(3), 3577–3585 (2017). https://doi.org/10.1016/j.proci.2016.07.074

Shinjo, J., Umemura, A.: Simulation of liquid jet primary breakup: dynamics of ligament and droplet formation. Int. J. Multiph. Flow **36**(7), 513–532 (2010). https://doi.org/10.1016/j.ijmultiphaseflow.2010.03.008

Shrimpton, J.: Charge injection systems: phycical principles, experimental and theoretical work (2009). https://doi.org/10.1007/978-3-642-002

Shum-Kivan, F., Santiago, J.M., Verdier, A., Riber, E., Renou, B., Cabot, G., Cuenot, B.: Experimental and numerical analysis of a turbulent spray flame structure. Proc. Combust. Inst. **36**(2), 2567–2575 (2017). https://doi.org/10.1016/j.proci.2016.06.039

Simmons, B.M., Agrawal, A.K.: Flow blurring atomization for low-emission combustion of liquid biofuels. Combust. Sci. Technol. **184**(5), 660–675 (2012). https://doi.org/10.1080/00102202.2012.660222

Singh, G., Kourmatzis, A., Gutteridge, A., Masri, A.R.: Instability growth and fragment formation in air assisted atomization. J. Fluid Mech. (2020). https://doi.org/10.1017/jfm.2020.179

Sovani, S., Sojka, P., Lefebvre, A.: Effervescent atomization. Prog. Energy Combust. Sci. **27**(4), 483–521 (2001). https://doi.org/10.1016/S0360-1285(00)00029-0

Turns, S.: An introduction to combustion: concepts and applications, 3rd edn. New York: McGraw-Hill (2012)

Tyliszczak, A., Cavaliere, D.E., Mastorakos, E.: LES/CMC of blow-off in a liquid fueled swirl burner. Flow Turbul. Combust. **92**(1), 237–267 (2014). https://doi.org/10.1007/s10494-013-9477-5

Varga, C.M., Lasheras, J.C., Hopfinger, E.J.: Initial breakup of a small-diameter liquid jet by a high-speed gas stream. J. Fluid Mech. **497**, 405–434 (2003). https://doi.org/10.1017/S0022112003006724

Verdier, A., Santiago, J.M., Vandel, A., Saengkaew, S., Cabot, G., Grehan, G., Renou, B.: Experimental study of local flame structures and fuel droplet properties of a spray jet flame. Proc. Combust. Inst. **36**(2), 2595–2602 (2017). https://doi.org/10.1016/j.proci.2016.07.016